Single-Crystal EPR of the ^{17}O-Enriched Dioxygen Adduct of Vitamin B_{12r}: Reversible Oxygen Bonding, Electronic and Geometric Structure, and Molecular Dynamics

E. Jörin,† A. Schweiger,* and Hs. H. Günthard

Contribution from the Laboratory for Physical Chemistry, Swiss Federal Institute of Technology, 8092 Zurich, Switzerland. *Received August 23, 1982*

Abstract: Single-crystal EPR studies on the oxygen adduct of vitamin B_{12r} and on the thermodynamics of the oxygenation process of B_{12r} were carried out on vitamin B_{12b} crystals doped with B_{12r} and $B_{12r}O_2$. For the determination of the spin density on the dioxygen, some of the crystals were enriched to about 25% in ^{17}O. EPR spectra of $B_{12r}O_2$ between −160 and 40 °C were recorded in three perpendicular planes defined by the crystallographic coordinate system *a,b,c* of the B_{12b} host crystal (space group $P2_12_12_1$). To eliminate the EPR signal of B_{12r}, which overlaps with the spectral features of $B_{12r}O_2$, the spectra of the latter were recorded at oxygen pressures up to 20 bar. At −160 °C, the **g** tensor and the two oxygen hyperfine tensors of $B_{12r}O_2$ are coaxial with the largest *g* principal axis along the O_α–O_β bond, whereas one of the principal axes of the cobalt hyperfine tensor is oriented approximately along the corrin normal. In this low-temperature modification the dioxygen molecule was found to be locked in a single minimum potential. The Co–O_α–O_β moiety was bent with a bond angle of 111°. The projection of the O_α–O_β direction on the corrin ring lies between rings B and C and approximately bisects the angle N22–Co–N23. The magnetic parameters of the low-temperature modification were discussed in detail within the spin-pairing and the superoxide formulation models. A total spin density on the dioxygen of $\rho_{O_2} = 0.7 \pm 0.1$ has been calculated. Drastic temperature-dependent changes in the **g** and $\mathbf{A}^{Co}$ tensors of $B_{12r}O_2$ with respect to axes directions and principal values were observed. Different models were discussed to interpret this temperature dependence. Most probably the dioxygen fragment is subject to a thermal motion described by an oscillation of O_β in a plane inclined to ring C, which is superimposed by a certain amount of wobbling. The thermodynamics of the solid-state oxygenation process $B_{12r} + O_2(g) \rightleftarrows B_{12r}O_2$ were studied in an oxygen pressure range of 0.20–20 bar and at temperatures between −160 and 40 °C. The pressure–temperature region for the reversibility of this process was found to be $-14 < T < 20$ °C and $p_{O_2} < 10$ bar. Enthalpy and entropy of this process were calculated to $\Delta H° = -6 \pm 1$ kcal/mol and $\Delta S° = -20 \pm 3$ cal/(mol·K), inferring a considerable mobility of O_2 in the B_{12r}–$B_{12r}O_2$ system.

Introduction

Reversible binding of dioxygen to synthetic Co(II) complexes has attracted much attention both from the point of view of the geometric and electronic structure of the dioxygen adduct and from the point of view of thermodynamics and kinetics of the sorption process.[1,2] From low-temperature X-ray structure analysis of several model compounds, a σ-bonded Co–O_2 moiety has been inferred.[3,4] At ambient temperature this technique indicates considerable disorder due to large-amplitude thermal motion of the Co–O_2 fragment and possibly other constituents of the complexes.[5-8] The electronic structure of oxygenated cobalt compounds has been studied extensively by EPR spectroscopy. In most of these investigations the magnetic parameters were interpreted in terms of a superoxo adduct of a Co(III) complex.[9] Recently a spin-pairing model has been proposed that leads to electron transfer from cobalt to O_2 ranging from zero to one.[10]

Reversible dioxygen adduct formation has also been observed with naturally occurring paramagnetic forms of vitamin B_{12}.[11-13] At present it is not known whether such $B_{12r}O_2$ adducts are important for the biological activity of the vitamin under physiological conditions. Earlier EPR studies of the $B_{12r}O_2$ system were carried out with powders[11] and frozen solutions,[11-13] which, however, did not afford a detailed insight into the electronic and geometric structure of the dioxygen adduct. Moreover, no thermodynamic data of the oxygenation process in the solid (single crystal) state are available.

In this paper we will report on an EPR study of vitamin B_{12r} and $B_{12r}O_2$ substituted in a B_{12b} single crystal. The following nomenclature for B_{12} derivatives based on the structural fragment shown in structure I[14] will be adopted.

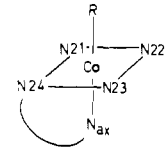

R = CN^-: vitamin B_{12} (cyanocob(III)alamin)
R = OH^-: vitamin B_{12b} (hydroxocob(III)alamin)
R = O_2: $B_{12r}O_2$ (oxygenated cobalamin)
R = -: five-coordinated B_{12r}

From the **g** tensor principal axes of B_{12r} obtained from EPR spectra of crystals in an inert atmosphere, the orientation of the B_{12r} molecule with respect to the crystal habit has been determined. Preliminary ENDOR data of B_{12r} from powders and single crystals provide further insight into the distribution of the unpaired electron on ligand nuclei. EPR spectra of $B_{12r}O_2$ have been recorded between −160 and 40 °C on crystals under 20 bar of oxygen. Under these conditions the oxygenation is complete, so that spectra of $B_{12r}O_2$ and B_{12r} no longer overlap. From the low-temperature data of the **g** and the ^{17}O hyperfine tensors, the geometrical structure of the Co–O_2 fragment will be determined and compared with structural data from corresponding model compounds. The

† Present address: Wild-Heerbrugg, CH-9435 Heerbrugg, Switzerland.

(1) (a) Jones, R. D.; Summerville, D. A.; Basolo, F. *Chem. Rev.* **1979**, *79*, 139-176. (b) Drago, R. S.; Corden, B. B. *Acc. Chem. Res.* **1980**, *13*, 353-360. (c) Drago, R. S.; Corden, B. B.; Zombeck, A. *Comments Inorg. Chem.* **1981**, *1*, 53-70. (d) Erskine, R. W.; Field, B. O. *Struct. Bonding (Berlin)* **1976**, *19*, 1-50.
(2) Smith, T. D.; Pilbrow, J. R. *Coord. Chem. Rev.* **1981**, *39*, 295-383.
(3) Gall, R. S.; Rogers, J. F.; Schaefer, W. P.; Christoph, G. G. *J. Am. Chem. Soc.* **1976**, *98*, 5135-5144.
(4) Avdeef, A.; Schaefer, W. P. *J. Am. Chem. Soc.* **1976**, *98*, 5153-5159.
(5) Rodley, G. A.; Robinson, W. T. *Nature (London)* **1972**, *235*, 438-439.
(6) Calligaris, M.; Nardin, G.; Randaccio, L.; Tauzher, G. *Inorg. Nucl. Chem. Lett.* **1973**, *9*, 419-422.
(7) Brown, L. D.; Raymond, K. N. *Inorg. Chem.* **1975**, *14*, 2595-2601.
(8) Huie, B. T.; Leyden, R. M.; Schaefer, W. P. *Inorg. Chem.* **1979**, *18*, 125-129.
(9) Hoffman, B. M.; Diemente, D. L.; Basolo, F. *J. Am. Chem. Soc.* **1970**, *92*, 61-65.
(10) Tovrog, B. S.; Kitko, D. J.; Drago, R. S. *J. Am. Chem. Soc.* **1976**, *98*, 5144-5153.
(11) Bayston, J. H.; King, N. K.; Looney, F. D.; Winfield, M. E. *J. Am. Chem. Soc.* **1969**, *91*, 2775-2779.
(12) Cockle, S. A.; Hill, H. A. O.; Williams, R. J. P. *Inorg. Nucl. Chem. Lett.* **1970**, *6*, 131-134.
(13) Schrauzer, G. N.; Lee, L. P. *J. Am. Chem. Soc.* **1970**, *92*, 1551-1556.
(14) For the complete vitamin structure and for the system of numbering the B_{12} atoms, see, for example: "B_{12}"; Dolphin, D., Ed.; Wiley-Interscience: New York, 1982; Vol. 1.

0002-7863/83/1505-4277$01.50/0

cobalt hyperfine structure will be discussed within the spin-pairing and the superoxide formation models. For $B_{12r}O_2$, direct rather than spin-polarization effects are found to be responsible for the cobalt hyperfine data. The magnetic parameters of $B_{12r}O_2$ in B_{12b} were found to exhibit a pronounced temperature dependence. Several models will be proposed that should serve as an explanation for the temperature effects. In order to assist some of the conclusions made in these models and to get an insight into the oxygenation process, the thermodynamics of the dioxygen adduct formation of B_{12r} in B_{12b} crystals is studied in an oxygen pressure range of 0.20–20 bar and at temperatures between −160 and 40 °C. From this study a pressure–temperature region for the reversibility of the oxygenation process in the solid state and the thermodynamic quantities $\Delta H°$ and $\Delta S°$ will be determined. Interpreting the latter enthalpy and entropy quantities, a considerable mobility of O_2 in the $B_{12r}O_2$ system is inferred.

Experimental Section

Materials. Vitamin B_{12b} and $NaBH_4$ were purchased from Fluka. Molecular oxygen (purity 99.998) was obtained from Messer Griesheim and used without further purification. Oxygen gas enriched with 25 atom % ^{17}O was purchased from Merck Sharp and Dohme Canada Ltd.

Growth of B_{12b} Single Crystals Doped with B_{12r}. B_{12b} instead of B_{12} was used as a host compound because of its higher solubility, which allows growth of single crystals of sufficient size for EPR and ENDOR investigations. Crystals were grown by the following two techniques:

(a) Growth was initiated from saturated aqueous B_{12b} solution (pH 9) in a prismatic glass container ($60 \times 60 \times 50$ mm^3) surrounded by an excess of liquid acetone in an exsiccator. It was found that using this type of container, the formation of irregularly shaped and dendrolitic crystals can be reduced. At room temperature the evaporated acetone diffuses slowly from the gas phase into the aqueous B_{12b} solution, thereby continuously decreasing the solubility of the latter. Long, needle-shaped single crystals of $1 \times 1 \times 20$ mm^3 dimension grow within 2–3 weeks. For the preparation of single crystals doped with B_{12r} the same procedure was applied, by using saturated aqueous solutions of B_{12r} (6%) and B_{12b} (94%) in an argon atmosphere. B_{12r} was prepared by reducing an aqueous solution of B_{12b} with $NaBH_4$ under anaerobic conditions.

(b) Growth of pure vitamin B_{12b} and mixed B_{12b}/B_{12r} single crystals was initiated from a saturated aqueous solution, carefully covered with a 10-fold excess of acetone in long glass tubes of 15 mm i.d. Polyhedron-shaped crystals with a maximum size of $2 \times 1.5 \times 1.5$ mm^3 grow within 5–6 weeks. In the mother liquor the crystals contain 25 H_2O molecules per B_{12b} molecule ("wet" modification). In contact with air the crystals lose seven water molecules per B_{12b} molecule ("dry" modification).[15] To reduce crack formation during the drying process, the crystals were left at −10 °C for several days. The "dry" B_{12b} crystals are orthorhombic with space group $P2_12_12_1$ and unit-cell dimensions a = 23.17 Å, b = 20.86 Å, and c = 15.83 Å. Each unit cell contains four molecules that are magnetically inequivalent.[16]

Instrumentation. EPR spectra were recorded on a Varian Model E-9 spectrometer equipped with a large sample cavity (Varian E235) and a homemade proton magnetometer. Concentrations of B_{12r} and $B_{12r}O_2$ were determined from double-integrated spectra digitized by a serializer system of our own design and processed by a data processing program PACKAGE developed by Dschen.[17] The ENDOR instrumentation has been published elsewhere.[18] ENDOR spectra were recorded between 8 and 20 K by using a Helitran gas-cooling system from Air Products and Chemical Inc. Temperature-variable $B_{12r}{}^{16}O_2$ single-crystal spectra and the oxygenation process were studied with a high-pressure EPR accessory designed for oxygen pressures up to 80 bar. The construction of the gas cell and the equipment used to produce and to control the O_2 pressure in the cavity are shown schematically in Figure 1. The high-pressure cell was made of a precision bore quartz tube of 6.0 mm o.d. and 3.0 mm i.d. (Wilmad Corp., NJ), mounted in a frame and connected to the gas control system through a high-pressure steel capillary. The whole system was made impervious to vacuum and pressure up to 100 bar by means of Viton O-rings. The quartz tube was mounted in a Dewar that provided cooling or heating of the sample within ±1 °C between −180 and 50 °C. Crystal holders were made of Plexiglass rods

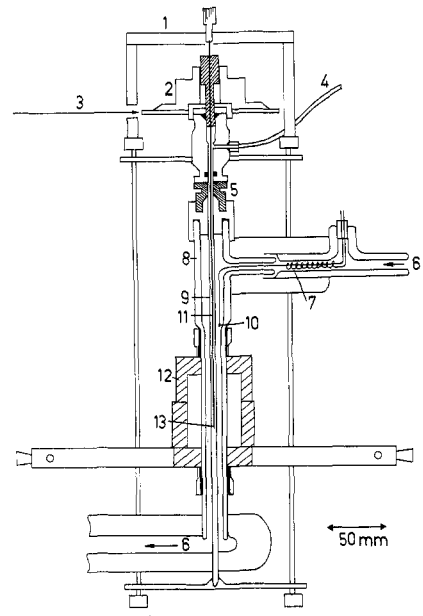

Figure 1. Schematic diagram of the high pressure EPR gas cell: (1) brass frame; (2) goniometer head; (3) laser beam for adjustment of reference plane; (4) stainless steel high-pressure capillary; (5) high-pressure gasket; (6) cold nitrogen gas inlet/outlet; (7) heater; (8) quartz Dewar; (9) high-pressure quartz tube; (10) thermocouple; (11) Plexiglass sample holder; (12) large access cavity; (13) sample (single crystal).

of 1.5-mm diameter. The lower end was shaped for the mounting of the single crystals. The upper end was cemented into a stainless steel tube, which served as mounting for the goniometer head and for gasketing of the crystal holder toward the high-pressure system. The O_2 gas pressure was measured by a calibrated mechanical manometer ($p \leq 160$ bar). To allow for slow pressure changes, the admission of O_2 gas from the pressure cylinder was made through needle valves. In order to protect the operator against oxygen explosion, the gas control system was equipped with a two-contact manometer that stops O_2 admission should the pressure be too high or on bursting of the quartz tube. A defined pressure–temperature condition was established by setting the temperature control unit and the gas pressure to preselected values. The system was then closed and allowed to reach a stationary O_2 pressure. Since measurements with the high-pressure setup required several hours, it was necessary to keep the water content of the "dry" crystals constant. This was achieved by adding a drop of water to the bottom of the quartz tube.

Preparation of $B_{12r}{}^{17}O_2$ samples required a modified technique owing to the restricted amount of ^{17}O-enriched O_2 gas available for this experiment. The crystal was mounted on a short crystal holder that was placed in a thick-walled quartz tube connected to a vacuum line. A volumetrically measured amount of ^{17}O-enriched O_2 gas was condensed into the quartz tube, which was then fused off and inserted into a conventional variable-temperature EPR setup.

Results

Magnetic Parameters of B_{12r}. The magnetic parameters of B_{12r} diluted in "dry" B_{12b} single crystals form one of the bases for characterization of the structure of the Co–O_2 moiety in $B_{12r}O_2$. X-band EPR spectra of B_{12r} were recorded between −120 and 20 °C for rotations of the B_{12b} crystal around the crystallographic axes a,b,c. The observed dependence of the line width on temperature, $m_I{}^{Co}$, and the orientation of B_0 have been discussed previously;[19] 20 °C is found to be an optimum temperature with respect to resolution of the spectra. For crystal settings with B_0 lying near the complex plane, the cobalt hyperfine splitting is only partially resolved. In addition, the EPR spectra of the four magnetically inequivalent sites only coincide for B_0 along a, b, and c. Due to these complications it was impossible to evaluate orthorhombic distortions of the **g** and $\mathbf{A}^{Co}$ tensors from X-band spectra. Q-band EPR spectra at 20 °C were measured for a crystal rotation around a, in order to determine the **g** tensor more accurately. Since this direction is approximately parallel to the

(15) Jörin, E.; Rist, G.; Schweiger, A.; Günthard, Hs. H. *Biochim. Biophys. Acta*, in press.
(16) Hodgkin, D. C.; Kamper, J.; Lindsey, J.; MacKay, M.; Pickworth, J.; Robertson, J. H.; Shoemaker, C. B.; White, J. G.; Prosen, R. J.; Trueblood, K. N. *Proc. R. Soc. London, Ser. A* **1957**, *242*, 228–263.
(17) Dschen, T. Thesis, Nr. 6799, ETH Zurich, 1981.
(18) Gruber, K.; Forrer, J.; Schweiger, A.; Günthard, Hs. H. *J. Phys. E* **1974**, *7*, 569–574.
(19) Schweiger, A.; Jörin, E.; Günthard, Hs. H. *Chem. Phys. Lett.* **1979**, *61*, 223–227.

Table I. Magnetic Parameters of B_{12r}[a]

		direction cosines[b,c]		
	principal values	*a*	*b*	*c*
g	$g_1 = 2.310 \pm 0.005$[d]	−0.324	−0.281	0.903
	$g_2 = 2.190 \pm 0.005$[d]	−0.232	−0.894	−0.383
	$g_3 = 2.004 \pm 0.005$[e]	0.917	−0.349	0.193
A^{Co}[f]	$A_1 = 65 \pm 12$			
	$A_2 = 80 \pm 12$			
	$A_3 = 302 \pm 10$			
A^{N}[f,g]	$A_1 = 45 \pm 2$			
	$A_2 = 45 \pm 2$			
	$A_3 = 53 \pm 2$			
Q^{N}[f,g]	$Q_1 = 0.85 \pm 0.1$			
	$Q_2 = 0.85 \pm 0.1$			
	$Q_3 = -1.70 \pm 0.1$			

[a] Doped in "dry" B_{12b} single crystals. [b] Direction cosines of the g tensor in site 1 (see ref 19, Figure 3) with respect to the crystallographic axes *a,b,c* of B_{12b}. [c] All the tensors are coaxial within error limits. [d] Q band. [e] X band. [f] In megahertz. [g] Benzimidazole nitrogen from powder ENDOR.

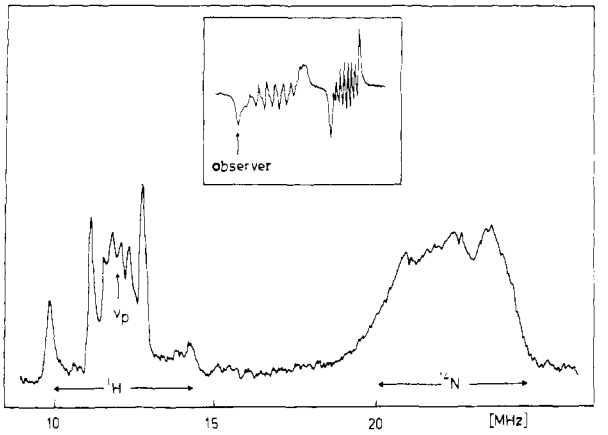

Figure 2. Single-crystal ENDOR spectrum of B_{12r} in B_{12b}: B_0 parallel to *b*, temperature 10 K; ν_p denotes proton Zeeman frequency. Insert: EPR spectrum of B_{12r} and $B_{12r}O_2$; arrow indicates EPR observer line.

complex normal (see discussion), B_0 rotates roughly in the complex plane.[20] In the Q-band EPR spectra the cobalt hyperfine structure is not resolved, however. The magnetic parameters of B_{12r} in B_{12b} single crystals are summarized in Table I.

ENDOR spectra from frozen H_2O–MeOH solutions of B_{12r}[21] and of B_{12r} doped B_{12b} single crystals with *c* parallel to the rotation axis yield the hyperfine and quadrupole tensor of the axially coordinated benzimidazole nitrogen as well as the approximate coupling parameters of some protons near the Co(II) ion. The single-crystal ENDOR spectrum for B_0 parallel to *a* with proton hyperfine splittings of 4.4, 1.6, and 0.8 MHz is shown in Figure 2. Nitrogen ENDOR parameters are collected in Table I. A complete evaluation of proton hyperfine tensors from ENDOR single-crystal data could not yet be obtained for reasons of spectrum complexity and signal to noise problems arising for crystal rotations around *a* and *b*.

Reversible Formation of $B_{12r}O_2$. The study of the solid-state oxygenation process of B_{12r} in "dry" B_{12b} crystals is based on relative spin concentration measurements of the B_{12r} and the $B_{12r}O_2$ EPR signals. The influence of the oxygen pressure on the degree of oxygenation is illustrated in Figure 3 for a temperature of 5 °C. At 0.2 bar of oxygen the EPR spectrum is dominated by the B_{12r} signal, whereas at 20 bar of O_2 complete conversion of B_{12r} to $B_{12r}O_2$ takes place within about 30 min.

Since the EPR spectra of B_{12r} and $B_{12r}O_2$ overlap for most of the crystal orientations, the suppression of the spectral features

(20) The deviation of *a* from the complex normal defined by g_3 has been considered in the determination of g_1 and g_2 from Q-band spectra.

(21) Jörin, E.; Graf, F.; Schweiger, A.; Günthard, Hs. H. *Chem. Phys. Lett.* **1976**, *42*, 376–379.

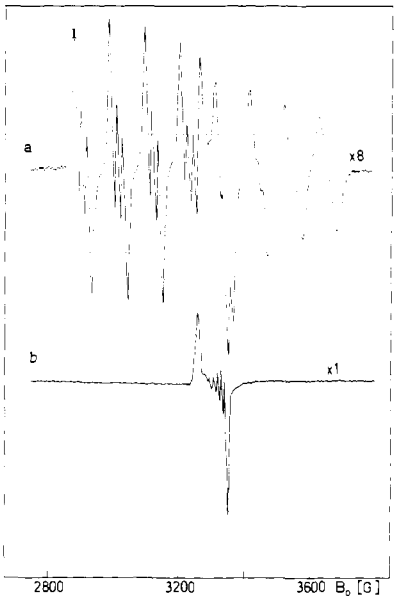

Figure 3. Effect of oxygen pressure on the intensity of the EPR spectrum of B_{12r}: (a) 0.20 bar of oxygen; spectrum of $B_{12r}O_2$ is overlapped by a strong B_{12r} signal; (b) 20 bar of oxygen; B_{12r} signal is completely eliminated.

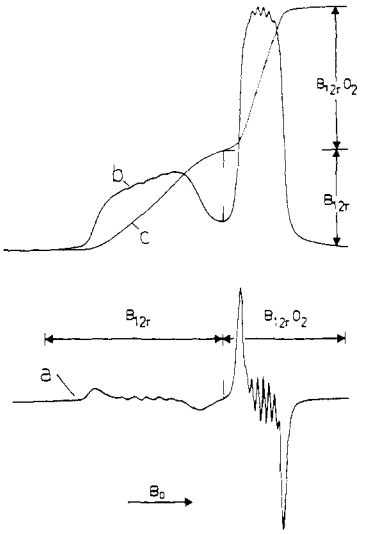

Figure 4. Determination of the concentration ratio $[B_{12r}O_2]/[B_{12r}]$ from single-crystal EPR spectra: (a) experimental EPR spectrum, first derivative of the absorption signal; (b) integrated EPR spectrum; (c) double-integrated EPR spectrum.

of B_{12r} at high oxygen pressure is an important prerequisite for an accurate measurement of the magnetic parameters of $B_{12r}{}^{16}O_2$ and $B_{12r}{}^{17}O_2$. $B_{12r}O_2$ may easily be transformed back to B_{12r} by putting the crystal in an argon atmosphere so that the EPR spectra of *both* B_{12r} and $B_{12r}O_2$ may be studied successively with the same crystal and the same setting.

The interconversion defined by eq 1 is found to be completely

$$B_{12r} + O_2(g) \rightleftharpoons B_{12r}O_2 \qquad (1)$$

reversible within the temperature interval $-14 < T < 20$ °C and for oxygen pressures up to 10 bar. At higher pressure and temperature, irreversible oxidation of the B_{12r} species occurs, whereas at $T < -14$ °C the $B_{12r}O_2$ formation becomes very slow.

For the evaluation of the thermodynamic data for the oxygen adduct formation, the crystals have been oriented with the *b* axis parallel to B_0. With this setting the EPR spectral features of B_{12r} and $B_{12r}O_2$ only slightly overlap (see Figure 4). This allows the determination of relative concentrations of the two paramagnetic species from double integration of digitized spectra. Since some overlap of the spectra persists even with this specific crystal setting,

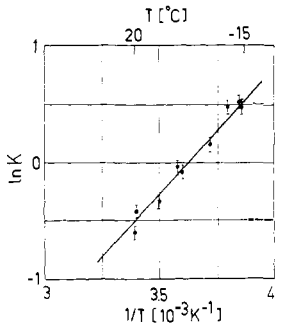

Figure 5. van't Hoff plot of the reversible oxygenation of B_{12r}; oxygen pressure 0.20 bar. Full circles denote experimental values.

the evaluation of relative intensities is subject to some uncertainty.

The equilibrium constant $K_1(p,T) = [B_{12r}O_2]/[B_{12r}]p_{O_2} = K/p_{O_2}$ for the process defined in eq 1 is obtained experimentally by the EPR intensity ratio (eq 2) and depends on the intensive variables

$$I_{B_{12r}O_2}/I_{B_{12r}} = [B_{12r}O_2]/[B_{12r}] \quad (2)$$

p,T according to

$$\ln K(p,T) = -\Delta H^\circ(p_0,T_0)/RT + \Delta S^\circ(p_0,T_0)/R + \ln (p/p_0) + B(p - p_0)/RT + D(p_0,T_0) \quad (3)$$

In the calculation of the K values the constancy of the sum $I_{B_{12r}O_2} + I_{B_{12r}}$ has been determined in each measurement of either isotherms or isobars. Constancy of this sum in loading and deloading cycles may be considered as a test for the reversibility of eq 1 and the lack of irreversible side reactions. Within the reversible pressure–temperature domain of the reaction, the last two terms in eq 3 may be neglected. From the van t'Hoff plot shown in Figure 5

$$\Delta H^\circ \text{ (1 bar, 273 K)} = -6 \pm 1 \text{ kcal/mol}$$

$$\Delta S^\circ \text{ (1 bar, 273 K)} = -20 \pm 3 \text{ cal/(mol·K)}$$

were obtained. From the isotherm representation of ln K vs. p, based on seven measurements with $0.2 < p_{O_2} < 10$ bar, the slope of ln K vs. ln p/p_0 amounts to 0.88 ± 0.12, confirming the expected behavior for the reaction in eq 1 within error limits.

Low-Temperature EPR Data of $B_{12r}O_2$. All the low-temperature (−160 °C) EPR spectra of $B_{12r}O_2$ have been measured at oxygen pressures between 10 and 30 bar, where complete oxygenation takes place. Since under these conditions only the spectrum of $B_{12r}O_2$ is observed, the angular dependence of three full rotations around the crystallographic axes a, b, and c could be studied. This allows a more accurate determination of the magnetic parameters than in preliminary work.[22] The angular dependences of **g** as well as the cobalt and ^{17}O hyperfine splittings for a rotation around c are depicted in Figure 6. For these crystal settings the spectra of site 1 and 3 and site 2 and 4 overlap.[22] The data collected in Table II refer to the same site as used in Table I. The assignment of the four $B_{12r}O_2$ sites to the four sites of B_{12r}, an important presumption for the discussion of the structure of the oxygen adduct, has been discussed earlier.[22,23] The assumption that the larger ^{17}O hyperfine coupling has to be assigned to O_β is based on a study of specifically ^{17}O-enriched peroxy radicals.[24] The **g** tensor and the ^{17}O hyperfine tensor of O_α and O_β are found to be coaxial within error limits. The principal axes of the cobalt hyperfine tensor, however, do not coincide with the axes of the **g** tensor. This is already demonstrated by the different positions of the extrema of the angular dependence of **g** and $\mathbf{A}^{Co}$ (see Figure 6). The absolute signs of the hyperfine principal values of cobalt and oxygen are based on theoretical predictions. In principle, they

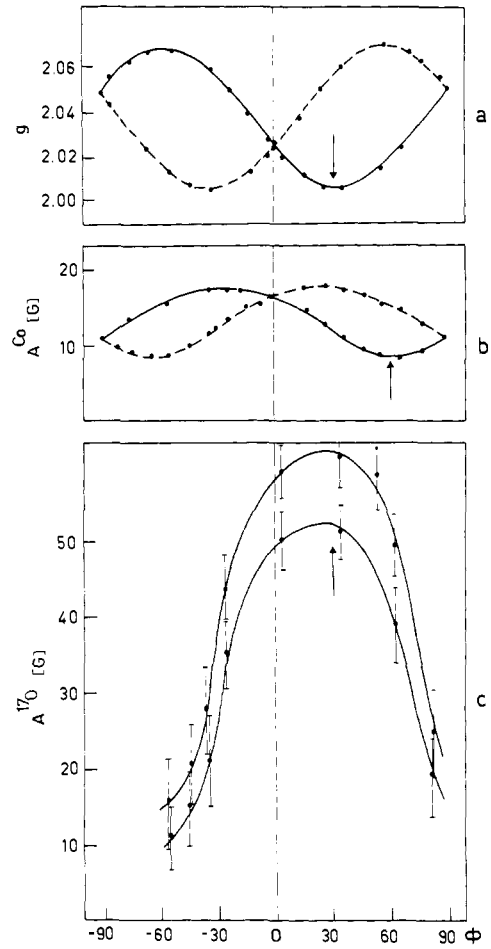

Figure 6. Angular dependence of the magnetic parameters of $B_{12r}O_2$ for a rotation around c; temperature −160 °C; full circles, experimental values; full lines, site 2 and 3; dashed lines, site 1 and 4. Arrows denote maxima or minima of the splittings of site 2 and 3: (a) Zeeman splitting; (b) cobalt hyperfine splitting; (c) ^{17}O hyperfine splitting.

Table II. Low-Temperature Parameters of $B_{12r}O_2$[a,b]

		direction cosines		
	principal values	*a*	*b*	*c*
g	$g_{x'} = 1.993 \pm 0.005$	0.104	0.621	0.777[c,d]
	$g_{y'} = 2.013 \pm 0.005$	0.719	−0.587	0.373
	$g_{z'} = 2.089 \pm 0.005$	0.687	0.519	−0.508
A^{Co}	$A_1 = -30.0 \pm 4$	−0.393	0.773	0.498
	$A_2 = -64.8 \pm 4$	−0.369	−0.629	0.684
	$A_3 = -18.7 \pm 4$	0.842	0.086	0.533
$A^{17}O_\alpha$	$A_{x'} = -167 \pm 8$			
	$A_{y'} = 59 \pm 10$			
	$0 < A_{z'} < 20$ (estimation)			
$A^{17}O_\beta$	$A_{x'} = -201 \pm 8$			
	$A_{y'} = 70 \pm 10$			
	$0 < A_{z'} < 20$ (estimation)			

[a] Temperature −160 °C, oxygen pressure 10 bar. [b] Hyperfine data in megahertz, calculated from the experimental values in gauss, by using the conversion formula A (MHz) = $2.8025(g_{eff}/g_e)A$ (gauss) and the orientation of the g tensor with respect to the A tensor. [c] Direction cosines of site 1 with respect to the crystallographic axes a,b,c. [d] Direction cosines of the ^{17}O hyperfine tensors coincide with the values for the g tensor.

can be determined experimentally from double ENDOR spectra by using a proton ENDOR line with a known m_S state as observer.[25] In the case at hand, however, the signal to noise ratio of the EPR spectra was by far too small for double ENDOR experiments. For the same reason, ^{17}O ENDOR spectra could not be observed.

(22) (a) Jörin, E.; Schweiger, A.; Günthard, Hs. H. *Chem. Phys. Lett.* **1979**, *61*, 228–232. (b) Jörin, E.; Schweiger, A.; Günthard, Hs. H. In "B_{12}"; ed. Dolphin, D., Ed.; Wiley-Interscience: New York, 1982; Vol. 1, pp 175–178.

(23) For site numbering with respect to the crystallographic axes see Figure 3 of ref 19.

(24) Howard, J. A. *Can. J. Chem.* **1972**, *50*, 1981–1983.

(25) Schweiger, A. *Struct. Bonding (Berlin)* **1982**, *51*, 1–122.

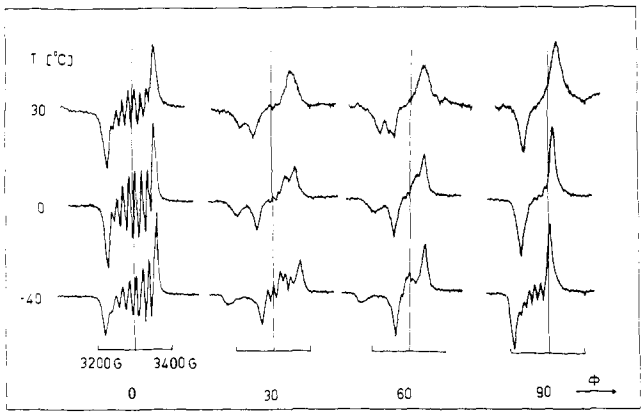

Figure 7. Temperature dependence of $B_{12r}O_2$ single-crystal EPR spectra; rotation around c. $\phi = 0$; B_0 is parallel to b.

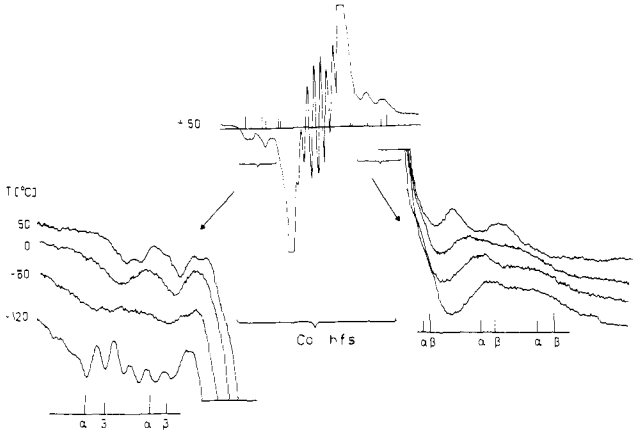

Figure 8. Temperature dependence of ^{17}O-enriched $B_{12r}O_2$ single-crystal EPR spectra. B_0 is parallel to b. α and β denote resonance lines of species $^{17}O_\alpha$–$^{16}O_\beta$ and $^{16}O_\alpha$–$^{17}O_\beta$ at −120 °C. Line positions (α,β) are calculated from the low-field $|m_I| = {}^5/_2$ position and the center of the $B_{12r}O_2$ spectrum.

Temperature Dependence of EPR Spectra of $B_{12r}O_2$. The single-crystal EPR spectra of $B_{12r}O_2$ show a pronounced temperature dependence. This is shown qualitatively for $B_{12r}{}^{16}O_2$ in Figure 7 and for $B_{12r}{}^{17}O_2$ in Figure 8. The EPR spectra of $B_{12r}{}^{17}O_2$ are superpositions of signals from the species $^{16}O_\alpha$–$^{16}O_\beta$ (56.3%), $^{16}O_\alpha$–$^{17}O_\beta$ (18.7%), $^{17}O_\alpha$–$^{16}O_\beta$ (18.7%), and $^{17}O_\alpha$–$^{17}O_\beta$ (6.0%). The anisotropy of all the magnetic parameters decreases with increasing temperature. Pronounced line-broadening effects, however, are observed only in ^{17}O-enriched $B_{12r}O_2$.

The **g** tensors were evaluated from three crystal rotations at five different temperatures. The temperature dependence of the **g** principal values is given in Figure 9a and Tables II and III. Up to −150 °C no change was observed in the spectral features; thus we define the structure represented by these data as the low-temperature modification. The most pronounced variation was found within the temperature range $-50 < T < 40$ °C. For $T > 50$ °C the **g** tensor approaches a constant high-temperature value. Spectra at temperatures higher than 60 °C could not be measured because of rapid irreversible oxidation of $B_{12r}O_2$. Parallel to the decrease in anisotropy with increasing temperature, the principal axes system of the **g** tensor was found to experience a rotation around an axis that nearly coincides with the largest g principal axis of the low-temperature modification. This rotation is described in Tables II and III by the direction cosines of the g principal axes or more directly by the rotation angle η shown in Figure 9d. An analogous change of principal values and axes directions is also observed for the cobalt hyperfine tensor (see Tables II and III). The orientation of the principal axes of g at −160 and 40 °C is shown in Figure 9d. The traces of the **g** and $\mathbf{A}^{Co}$ tensors are found to be temperature independent within error limits. A considerable decrease of anisotropy with increasing temperature has likewise been found for the ^{17}O hyperfine tensors.

Table III. High-Temperature Magnetic Parameters of $B_{12r}O_2$[a]

		direction cosines[b]		
	principal values	*a*	*b*	*c*
g	$g_x'^{av} = 2.009 \pm 0.006$	0.481	0.224	0.848
	$g_y'^{av} = 2.023 \pm 0.006$	0.477	−0.878	−0.039
	$g_z'^{av} = 2.049 \pm 0.006$	0.736	0.423	−0.529
A^{Co}[c]	$A_x'^{av} = -37.4 \pm 6$	0.014	0.647	0.762
	$A_y'^{av} = -47.4 \pm 6$	−0.265	−0.733	0.627
	$A_z'^{av} = -25.2 \pm 6$	0.964	−0.210	0.161

[a] Temperature 40 °C. [b] Direction cosines of site 1 with respect to the crystallographic axes a,b,c. [c] In megahertz.

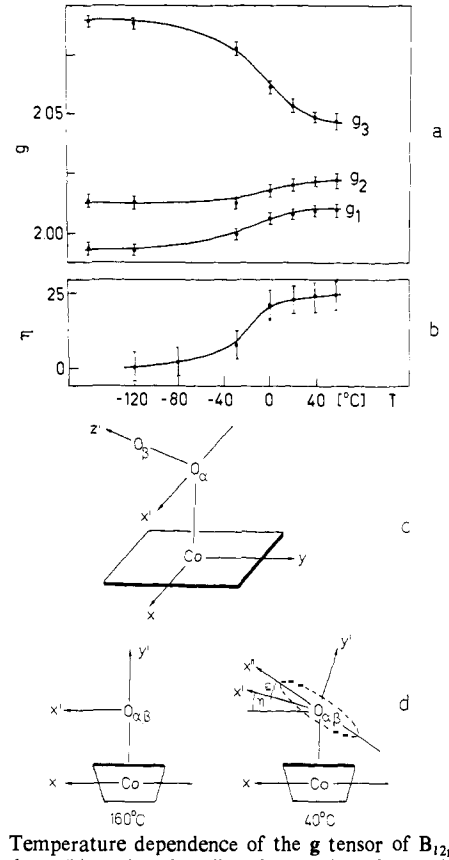

Figure 9. Temperature dependence of the **g** tensor of $B_{12r}O_2$: (a) **g** principal values; (b) angle η describes the rotation of the principal axes of g_x^{av} and g_y^{av} around O_α–O_β with respect to the local coordinate system x',y',z' at −160 °C. (c) Schematic representation of the low-temperature configuration (for details, see Figure 10); (d) orientation of the **g** principal axes system defined by x',y',z' at −160 and 40 °C. View along O_α–$O_\beta(z')$. Dashed curve gives a qualitative hint of the disorder of O_β described by the wobbling-oscillation model.

However, it was not possible to obtain quantitative data because of poor signal intensity and the smaller ^{17}O splittings at higher temperatures.

Discussion

Definition of Reference Frames. Different coordinate systems will be used in the characterization and interpretation of the magnetic data. The orientation of the orthogonal crystallographic axes a,b,c of the unit cell of "dry" B_{12b} is well determined by the crystal habit.[26] All the direction cosines of the tensors of, say, site 1 in Tables I–III refer to this coordinate system. Since no X-ray data of B_{12b} are available, the orientation of the molecular coordinate system of B_{12b} with respect to a,b,c has been calculated from B_{12} X-ray data of dry crystals[27].

The B_{12} coordinate system is defined by axis y, which bisects the N21–Co–N24 angle, by axis x perpendicular to y and lying

(26) Hodgkin, D. C. *Prog. Chem. Org. Nat. Prod.* **1958**, *15*, 167–218.
(27) Hodgkin, D. C.; Lindsey, J.; Sparks, R. A.; Trueblood, K. N.; White, J. G. *Proc. R. Soc. London, Ser. A* **1962**, *266*, 494–517.

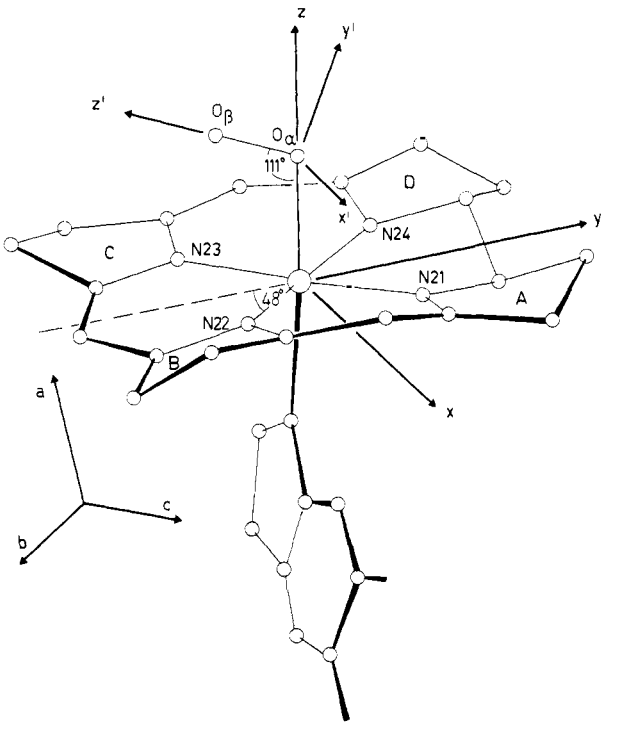

Figure 10. Low-temperature geometry of a fragment of $B_{12r}O_2$. Atomic positions of B_{12r} are taken from the X-ray structure of "dry" B_{12} crystals:[27] *a,b,c*, crystallographic system; *x,y,z*, molecular system; *x',y',z'*, coordinate system defined by the **g** principal axes at −160 °C.

in the least-squares plane through the equatorial nitrogen ligands, and by axis *z* normal to this plane. From theoretical arguments the principal axis direction belonging to g_3 is expected to be parallel to the molecular *z* axis of B_{12r}. This prediction[28] has been verified from single-crystal EPR studies of different types of five coordinated cobalt low-spin complexes.[29,30] In addition, the complex normals *z* of B_{12b}, B_{12r}, and $B_{12r}O_2$ are assumed to be parallel. From comparison of the X-ray results of B_{12} and the direction of the g_3 principal axis of B_{12r}, an angle of 6° between $z(B_{12})$ and $z(B_{12r})$ has been found.[19] Considering this slightly different orientation of B_{12r} (B_{12b}) in the coordinate system *a,b,c*, the molecular frame *x,y,z* is defined by the basis transformation

$$(e_x,e_y,e_z) = (e_a,e_b,e_c)\mathbf{D} \qquad (4)$$

with

$$\mathbf{D} = \begin{bmatrix} -0.320 & -0.237 & 0.917 \\ 0.488 & -0.800 & -0.348 \\ 0.812 & 0.551 & 0.193 \end{bmatrix}$$

The cobalt 3d orbitals will be referred to this molecular frame.

The second local coordinate system *x',y',z'* is defined by the temperature-dependent **g** tensor principal axes system of $B_{12r}O_2$. Thereby the O_α–O_β bond direction at low temperature is assumed to lie parallel to the $g_{z'}$ direction.[31,32] This assumption is supported by the axes directions of the ^{17}O hyperfine tensors, which are defined essentially by the orientation of the $p_{x'}$ orbitals and which coincide with the **g** tensor axes. A further coordinate system (*x''*, *y'',z''*) is used in connection with the dioxygen disorder model with *z''* parallel to *z'* and the *x'',z'* plane defining the oscillation plane of O_β. The coordinate systems (*a,b,c*), (*x,y,z*), and (*x',y',z'*) at −160 °C are shown in Figure 10.

Table IV. Thermodynamic Data for the Oxygenation Reaction of Some Cobalt Complexes

$$Co(L_4)(B) + O_2 \rightleftarrows Co(L_4)(B)O_2$$

complex[a]	conditions	$\Delta H°$, (298),[b] kcal/mol	$\Delta S°$,[b] cal/(mol·K)	ref
Co(salen)	Me_2SO, soln	−16	−28	1
Co(acacen)(py)	toluene, soln	−17	−60	1
Co(T(*p*-OCH_3)PP)(py)	toluene, soln	−9	−42	1
Co(PP1XDME)(py)	toluene, soln	−9	−40	1
Co(TpivPP)(me-imid)	toluene, soln	−12	−38	33
Co(TpivPP)(me-imid)	solid	−13	−40	33
CoMb	soln, pH 7	−12	−35	1
CoHb	soln, pH 7	−8	−22	1
B_{12r}	solid	−6	−20	this work

[a] Abbreviations are from given in 41. [b] Standard state, 1 atm of O_2.

Thermodynamics of Reversible Dioxygen Bonding. For oxygen gas, the term $B(p - p_0)/RT$ in eq 3 can be neglected, since at p_{O_2} = 20 bar, it only contributes 0.03 to ln *K*. Furthermore, term *D* in eq 3 can be omitted in the small temperature range 278 ± 15 K. Hence a linear dependence of ln $K(p,T)$ vs. $1/T$ and ln p/p_0 is expected (see Figure 5).

In Table IV $\Delta H°$ and $\Delta S°$ of a number of cobalt oxygen carriers are collected.[1,33] The surprisingly low value of $\Delta S° \approx -20 \pm 3$ cal/(mol·K) found in this work should be noted. Values of $\Delta S° \approx -40$ cal/(mol·K) may be considered to result from loss of three translational and two rotational degrees of freedom in the sorption process of O_2. The value observed for the B_{12r}–$B_{12r}O_2$ system, however, corresponds to a loss of two translational degrees of freedom at the most, i.e., approximately one translational degree of freedom persists in the $B_{12r}O_2$ state. This indicates a considerable mobility of O_2, which probably relates to translational motion along the channels of the crystal water parallel to *c* found by X-ray analysis,[27] thus allowing only diffuse location of some (ca. five) of the H_2O molecules. Likewise, the $\Delta H°$ value obtained for reaction 1 appears small (see Table IV) in comparison to that for other Co–O_2 compounds. One exception is cobaltohemoglobin, which shows a $\Delta H°$ value similar to the one found in the B_{12r}–$B_{12r}O_2$ system. Closely analogous thermodynamic behavior for the crystal water has been found from thermal analysis.[15]

Electronic Structure of B_{12r}. EPR spectra of randomly oriented B_{12r} have been reported by several authors.[34-37] The spectra are interpreted in terms of a low-spin Co(II) $3d^7$ configuration with the unpaired electron in a ground state with dominant d_{z^2} character. Thus, the g_3 axis is assumed to be oriented parallel to the complex normal. The best resolved spectra are obtained from B_{12} reduced within the enzyme ribonucleotide reductase.[37] These spectra have been computer simulated by Pilbrow and Winfield[38] using monoclinic symmetry. They found that the axis of the **g** and the cobalt hyperfine tensor in the complex plane are noncoincident but are rotated by 50° with respect to each other. For theoretical reasons they assume the principal axes of g_1 and g_2 to lie roughly between the metal–ligand bond directions. Their principal values $g_1 = 2.295$, $g_2 = 2.230$, and $g_3 = 2.009$ evaluated

(28) Hitchman, M. A. *Inorg. Chem.* **1977**, *16*, 1985-1993.
(29) Chien, J. C. W.; Dickinson, L. C. *Proc. Natl. Acad. Sci. U.S.A.* **1972**, *69*, 2783-2787.
(30) Jörin, E.; Rudin, M.; Schweiger, A.; Günthard, Hs. H. *Chem. Phys. Lett.* **1980**, *69*, 193-197.
(31) Känzig, W.; Cohen, M. H. *Phys. Rev.* **1959**, *3*, 509-510.
(32) Chien, J. C. W.; Dickinson, L. C. "Biological Magnetic Resonance"; Berliner, L. J.; Reuben, J. Eds.; Plenum Press: New York, 1981; Vol. 3, pp 155-211.
(33) Collman, J. P.; Brauman, J. I.; Doxsee, K. M.; Halbert, T. R.; Hayes, S. E.; Suslick, K. S. *J. Am. Chem. Soc.* **1978**, *100*, 2761-2766.
(34) Schrauzer, G. N.; Lee, L. P. *J. Am. Chem. Soc.* **1968**, *90*, 6541-6543.
(35) Bayston, J. H.; Looney, F. D.; Pilbrow, J. P.; Winfield, M. E. *Biochemistry* **1970**, *9* 2164-2172.
(36) Cockle, S. A.; Hill, H. A. O.; Pratt, J. M.; Williams, R. J. P. *Biochim. Biophys. Acta* **1969**, *177*, 686-688.
(37) Hamilton, J. A.; Yamada, R.; Blakley, R. L.; Hogenkamp, H. P. C.; Looney, F. D.; Winfield, M. E. *Biochemistry* **1971**, *10*, 347-355.
(38) Pilbrow, J. R.; Winfield, M. E. *Mol. Phys.* **1973**, *25*, 1073-1092.

Table V. Structures of σ-Bound Cobalt Dioxygen Adducts

complex[a]	method	Co–O–O angle, deg	dihedral angle between Co–O–O and plane spanned by axial base, deg	T, °C	type of disorder	ref
Co(acacen)(py)(O_2)	X-ray	NA[b]	~90	−40	2-fold disorder of O_2 in a plane	6
Co(bzacen)(py)(O_2)	X-ray	126	~90	RT[c]	high thermal motion of O_2, single minimum	5
$Co(CN)_5(O_2)^{3-}$	X-ray	153		RT	2-fold disorder of O_α and O_β	7
Co(*t*-Bsalten)(bzl-imid)(O_2)	X-ray	117.5	18.5	−152	single minimum	3
Co(3-*t*-Bu-Salen)(py)(O_2)	X-ray	116.4	18	RT	single minimum	49
Co(3-MeO-Saltmen)aquo	X-ray	117		RT	2-fold disorder	8
Co(3-F-Saltmen)(1-me-imid)-(O_2)·2(CH_3)$_2$CO	X-ray	117.4	12.6	−171	single minimum	4
Co(Saltmen)(bzl-imid)(O_2)	X-ray	120	19.2	−18	single minimum	50
[Co(Salpeen)(O_2)]MeCN[d]	X-ray	134	~0	RT	high thermal motion of O_2, single minimum	51
oxycobaltomyoglobin	X-ray	131	NA	−20	single minimum	52
	EPR	−120[f]		−195	two Co–O_2 species	44
	EPR	108,[e,g] 111[f,g]	12, 40	−195	two Co–O_2 species	45
	EPR	129[g]	~60	RT	single minimum	45
$B_{12r}O_2$	EPR	111	86	−160	single minimum	*h*
	EPR	111[i]	86[i]	40	oscillation and wobbling of O_β	*h*

[a] For abbreviations see ref 41. [b] Not available. [c] Room temperature. [d] Pyridyl plane bisects the N–Co–N in-plane angle. [e] Species I. [f] Species II. [g] Co–O_α parallel to A_1^{Co}. [h] This work. [i] Averaged value.

from the simulated spectra are similar to the single-crystal Q-band data of B_{12r} in B_{12b} (see Table I). In the host compound at hand, however, the principal axis direction of g_1 is found to point approximately along N21 (deviation 13°). An extensive theoretical study for the interpretation of the EPR data of low-spin Co(II) complexes has been presented by McGarvey.[39] Since our B_{12r} EPR data mainly serve for the definition of the z axis of the molecular coordinate system, they will not be interpreted in more detail. For an extensive discussion of the magnetic parameters of cobalamins and cobinamides, the reader is referred to a review article published very recently by Pilbrow.[40]

From powder ENDOR data the largest principal axis of the axial nitrogen hyperfine tensor is found to point along the complex normal.[21] The spin densities in the σ-bond of N_{ax} are $\rho_{2s} = 0.031$ and $\rho_{2p} = 0.056$, resulting in a hybridization parameter of $n^2 = 0.63$, which is near the value for a sp^2 hybrid. The quadrupole coupling e^2qQ is calculated to be −3.27 MHz. These results are in close agreement with the corresponding parameters of the pyridine nitrogen in the model compound Co(salen)(py).[30,41]

ENDOR signals from the corrin nitrogen in B_{12r} could not be observed for several reasons. In the model compound Co(acacen) the nitrogen ENDOR transitions at low frequencies are about 10 times lower in intensity than the proton lines.[42] This is due to the small g_N^2 value in the expression for the nuclear transition probability. In B_{12b}/B_{12r} the disorder of the crystal which broadens the weak ENDOR lines leads to a further decrease in intensity. This is demonstrated in Figure 2 by the unexpected broad single-crystal nitrogen transitions of the axial base (four transitions), which should be compaired with the powder ENDOR line widths of 600 kHz for the pyridine nitrogen in Co(salen)(py).[30] Due to the restricted availability of proton ENDOR data, an assignment of the observed transitions to particular protons is not possible.

Low-Temperature Conformation of $B_{12r}O_2$. Evaluation of the structure of $B_{12r}O_2$ from X-ray diffraction analysis appears troublesome because of the difficult growth of pure B_{12r} crystals and their study under high oxygen pressure at low temperature.

EPR crystallography is occasionally a valuable alternative method for obtaining structural information on paramagnetic compounds. In this technique, the fact is used that magnetic interactions like Zeeman and hyperfine are tensorial quantities. These tensors can be used to extract geometrical information about the closer vicinity of the unpaired electron. In general, EPR and especially ENDOR crystallography may be used for an accurate determination of atomic parameters from electron-nuclear dipole interactions.[42,43] In $B_{12r}O_2$ the structural data obtained from the low-temperature EPR spectra are restricted to relations between the orientation of the Co–O_2 moiety and the molecular frame x,y,z. Statements about distances, however, cannot be made.

At −160 °C only one $B_{12r}O_2$ spectrum is observed for each crystal site, hence the dioxygen ligand is locked in a *single minimum potential*. Only a few low-temperature structures of cobalt oxygen carriers obtained from X-ray and EPR data are known.[3,4,44,45] From the X-ray data of cobalt Schiff base complexes, a well-defined single orientation of the terminal oxygen has been found,[3,4] whereas from EPR studies in oxycobaltomyoglobin two distinct forms with different orientations of the dioxygen molecule are observed.[44,45]

On the basis of the assumptions that g_z lies parallel to the O_α–O_β direction and that the Co–O_α bond is oriented normal to the corrin plane (parallel to z), the bond angle for the fragment Co–O_α–O_β is found to $\theta = 111°$. This value is close to the angle expected for an sp^2-hybridized adjacent oxygen atom, which is σ-bonded to cobalt. As shown in Table V this value for the Co–O_α–O_β bond angle fits well with that of a number of related cobalt dioxygen adducts. Similar data have also been found from computer-sim-

(39) McGarvey, B. R. *Can. J. Chem.* **1975**, *53*, 2498–2511.

(40) Pilbrow, J. R. In "B_{12}"; Dolphin, D., Ed.; Wiley-Interscience: New York, 1982; Vol. 1, pp 431–462.

(41) Abbreviations in this paper are as follows: Co(salen), [*N*,*N*′-ethylenebis(salicylideneaminato)]cobalt(II); Co(bzacen), [*N*,*N*′-ethylenebis(benzoylacetoneiminato)]cobalt(II); Co(acacen), [*N*,*N*′-ethylenebis(acetylacetone iminato)]cobalt(II); Co(*t*-Bsalten), [*N*,*N*′-(1,1,2,2-tetramethyl)-ethylenebis(3-*tert*-butylsalicylideneaminato)]cobalt(II); Co(3-F-Saltmen), [*N*,*N*′-(1,1,2,2-tetramethyl)ethylenebis(3-fluorosalicylideneaminato)]cobalt(II); Co^{II}(tspc), cobalt(II) tetrasulfonated phthalocyanine; Co(Salpeen), [*N*,*N*′-(2-(2′-pyridylethyl))ethylenebis(salicylideneaminato)]cobalt(II); Co(Saltmen), [*N*,*N*′-(1,1,2,2-tetramethyl)ethylenebis(salicylideneaminato)]cobalt(II); Co(3-*t*-Bu-Salen), [*N*,*N*′-ethylenebis(3-*tert*-butylsalicylideneaminato)]cobalt(II); Co(3-OMe-Saltmen), [*N*,*N*′-(1,1,2,2-tetramethyl)-ethylenebis(3-methoxysalicylideneaminato)]cobalt(II); Co(DMGH)$_2$, cobalt(II) dimethylglyoxime; Co(T(*p*-OCH_3)PP), cobalt(II) mesotetra(*p*-methoxyphenyl)porphyrinate; Co(PPIXDME), cobalt(II) protoporphyrinate IX dimethyl ester; Co(TpivPP), cobalt(II) (mesotetra($\alpha,\alpha,\alpha,\alpha$-*o*-pivalamidophenyl)porphyrinate; CoMb, cobalt(II) myoglobin, CoHb, cobalt(II) hemoglobin; py, pyridine; 1-bzl-imid, 1-benzylimidazole; 1-me-imid, 1-methylimidazole.

(42) Rudin, M.; Schweiger, A.; Günthard, Hs. H. *Mol. Phys.* **1982**, *46*, 1027–1044.

(43) Hutchison, C. A.; McKay, D. B. *J. Chem. Phys.* **1977**, *66*, 3311–3330.

(44) Dickinson, L. C.; Chien, J. C. W. *Proc. Natl. Acad. Sci. U.S.A.* **1980**, *77*, 1235–1239.

(45) Hori, H.; Ikeda-Saito, M.; Yonetani, T. *Nature (London)* **1980**, *288*, 501–502.

ulated frozen solution spectra.[46-48] The $p_{x'}$ orbitals of the two oxygens and the $g_{x'}$ principal axis direction are nearly parallel to the corrin plane. This is a strong indication that the plane of the Co–O_α–O_β moiety is oriented perpendicular to the latter. The projection of the O_α–O_β bond on the complex plane includes an angle of 48° with the Co–N22 direction, whereas the dihedral angle between the plane of the axial benzimidazole base and Co–O_α–O_β is 86°. The low-temperature structure of $B_{12r}O_2$, evaluated from single-crystal EPR data, is shown in Figure 10. From X-ray analysis on vitamin B_{12} it is known that the plane of the axial base and the molecular xz plane nearly coincide, i.e., the three planes formed by the equatorial nitrogens, the Co–O_α–O_β fragment, and the axial base are approximately perpendicular to each other. Such a geometrical configuration maximizes the overlap of the oxygen $\pi^*(x')$ orbital with the cobalt $3d_{xz}$ orbital (maximum π-back-bonding) and minimizes interaction of the benzimidazole ligand with the atoms in the corrin ring. This arrangement of the two axial ligands is strikingly similar to that of Co(bzacen)(py)(O_2)[5] and Co(acacen)(py)(O_2)[6] (see Table V). Therefore, in $B_{12r}O_2$ electronic effects seem to be more important for the relative orientation of the axial ligands than steric hindrance by side chains and crystal water molecules. This is in contrast to low-temperature structures of Co(*t*-Bsalten)(1-bzl-imid)(O_2)[3] and Co(3-F-Saltmen)(1-Me-Imid)(O_2)·2($(CH_3)_2CO$),[4] where strong steric constraints result in dihedral angles of 18.5 and 12.6°, respectively.

Electronic Structure of $B_{12r}O_2$. The magnetic parameters of $B_{12r}O_2$ at −160 °C are very similar to those found for a large number of oxygenated Co(II) complexes.[1,46] The electronic structure of this type of compound is usually discussed in terms of the superoxide formulation introduced by Hoffman et al.[9] or by the spin-pairing model proposed recently by Tovrog et al.,[10] which interprets the cobalt hyperfine structure as originating essentially from indirect spin-polarization contributions.

In the spin-pairing model, two relevant MO's of the Co–O_2 fragment, ψ_1 and ψ_2, affect the cobalt hyperfine interaction. The

$$\psi_1 = \alpha' d_{z^2} + \gamma 4s + \beta\pi^*(y') \quad (5)$$

$$\psi_2 = \epsilon\pi^*(x') + \alpha'' d_{xz} \quad (6)$$

doubly occupied σ MO describes the overlap of a $\pi^*(y')$ orbital of O_2 with the metal $3d_{z^2}$ and 4s orbital. The second MO with the O_2 orbital $\pi^*(x')$ contains the unpaired electron. Because ψ_1 and ψ_2 are close in energy,[10] ψ_2 can polarize ψ_1, i.e., negative spin density will be found in $3d_{z^2}$ and 4s.

Hoffman et al.[9] on the other hand propose a direct mechanism (π-back-bonding) for the description of the anisotropic cobalt hyperfine structure with the unpaired electron essentially located in a MO involving the antibonding $\pi^*(x')$ oxygen MO and the cobalt $3d_{xz}$ orbital. Since $\alpha''^2 \leq 0.1$ is found for a large number of cobalt dioxygen adducts with this model ($\alpha' = \gamma = 0$), almost complete electron transfer from cobalt to oxygen is concluded, leading to the superoxo formulation. Tovrog et al.[10] suggest that this π-back-bonding mechanism or direct delocalization of the unpaired electron into $3d_{xz}$ is of minor importance for most Co–O_2 compounds ($\alpha''^2 \leq 0.02$).

The spin-pairing model has recently been modified by Smith et al.,[47] who considered the cobalt orbital $3d_{yz}$ in ψ_1 by introducing the term $\alpha'''d_{yz}$ in eq 5. Including π-back-bonding (d_{xz}) in ψ_2 and the orbital d_{yz} in ψ_1, the principal values of the cobalt hyperfine tensor are given by eq 7, where $A_xA_yA_z$ denote the principal values

$$A_x - a_{Co} = \tfrac{2}{7}(f + g + 2h)$$

$$A_y - a_{Co} = \tfrac{2}{7}(f - 2g - h)$$

$$A_z - a_{Co} = \tfrac{2}{7}(-2f + g - h) \quad (7)$$

along x, y and z and a_{Co} is the isotropic hyperfine coupling constant. The expressions[53] $f = P\rho_O U_{Co-O}\alpha'^2$, $h = P\rho_O U_{Co-O}\alpha'''^2$, and $g = P\alpha''^2$ describe indirect spin polarization of d_{z^2} and d_{yz} and direct hyperfine contribution from d_{xz}, respectively, with the spin-polarization constant U_{Co-O}, the spin density ρ_O on the adjacent oxygen, and $P = g_e\beta_e g_n\beta_n\langle r^{-3}\rangle_{3d}$.

In a series of cobalt dioxygen adducts, including the extensively studied compounds Co(acacen)(py)(O_2) and Co(DMGH)$_2$(py)(O_2), Tovrog et al.[10] found that the cobalt hyperfine structure can be described by the spin-pairing model. However, in the interpretation of their frozen-solution data these authors have chosen the axis of the largest (negative) principal value along the complex normal z, so that polarization of d_{z^2} makes the main contribution to the cobalt hyperfine structure. This choice of the axis direction is in contradiction to the findings in the single-crystal EPR studies in this work and in oxycobaltomyoglobin,[44] which state that the largest component $A_1^{Co} = A_{max}^{Co}$ lies near the line intersecting the complex plane and the plane spanned by the Co–O–O fragment (90° in $B_{12r}O_2$). The same direction of A_{max}^{Co} has been found by Smith and co-workers[46-48] from frozen-solution spectra, for a large variety of cobalt dioxygen adducts using extensive computer simulation. Although conclusions drawn from simulations of randomly oriented paramagnetic species with symmetry lower than orthorhombic should be treated with care, an orientation of the cobalt hyperfine tensor with A_{max}^{Co} parallel to z can be excluded.

Calculation of numerical values for f, g, and h for $B_{12r}O_2$ (see eq 7) requires correction of the cobalt hyperfine data given in Table II for direct point dipole–dipole interaction between the unpaired electron on O_2 and the cobalt nucleus. For this coupling we use a value of $T_\parallel^{dip} = 3$ MHz.[10] Furthermore we assume $T_\parallel^{dip}$ to lie along z and the three experimental principal axes of A^{Co} to coincide with the molecular coordinate system x,y,z. Insertion of the corrected cobalt hyperfine data in eq 7 yields $f + h = -7.93$ MHz and $g + h = 40.60$ MHz. The positive value for $f + h$ calculated by Smith and Pilbrow[2] from the data published by Jörin et al.[22] arises from an incorrect assignment of tensor principal axes by these authors. Thus, all conclusions[2] made with respect to the positive sign have to be rejected. For $f + h < 0$, at least one of the two parameters has to be negative, implying direct interaction rather than spin polarization of d_{z^2} or d_{yz}. Unfortunately, it is not possible to extract individual values of f, g, and h. Assuming $h \leq 0$ and a reduced P value of 600 MHz, $\alpha''^2 \geq 0.07$ is obtained, which (neglecting two-center integrals) is equal to the spin density $\rho_{d_{xz}}$. This direct delocalization of unpaired spin is considerably larger than suggested by Tovrog et al.[10] and represents the principal contribution to the anisotropic cobalt hyperfine structure in $B_{12r}O_2$.

Within the frame of the spin-pairing model, the quantity $f + h$ has to be positive. Since for $B_{12r}O_2$ and a large number of synthetic Co–O_2 adducts[2] $f + h$ is found to be negative, the model appears incomplete to describe the cobalt hyperfine structure of these types of compounds. Our finding, however, does not necessarily conflict with the statement that the extent of electron transfer into O_2 might be small. It only implies that the cobalt hyperfine tensor may not fully be explained by polarization of the spins in the ψ_1 orbital. This anisotropic hyperfine coupling is described by $U_{Co-O}\rho_O\alpha'^2A_{aniso(3d)}$, where $A_{aniso(3d)}$ denotes the (reduced) anisotropy for one full electron in a 3d orbital. Since both α'^2 and U_{Co-O} are unknown in this expression, α'^2 and thus the electron transfer defined by $2(1 - \alpha'^2) - 1$ cannot be determined from EPR data. By use of the finite spin-polarization

(46) Ruzic, I. M.; Smith, T. D.; Pilbrow, J. R. *J. Chem. Soc., Dalton Trans.* **1981**, 2365–2369.
(47) Smith, T. D.; Ruzic, I. M.; Tiraut, S.; Pilbrow, J. R. *J. Chem. Soc., Dalton Trans.* **1982**, 363–372.
(48) Ruzic, I. M.; Smith, T. D.; Pilbrow, J. R. *J. Chem. Soc., Dalton Trans.* **1982**, 373–380.
(49) Schaefer, W. P.; Huie, B. T.; Kurilla, M. G.; Ealick, S. E. *Inorg. Chem.* **1980**, *19*, 340–344.
(50) Gall, R. S.; Schaefer, W. P. *Inorg. Chem.* **1976**, *15*, 2758–2763.
(51) Jameson, G. B.; Robinson, W. T.; Rodley, G. A. *J. Chem. Soc., Dalton Trans.* **1978**, 191–196.
(52) Petsko, G. A.; Rose, D.; Tsernoglou, D.; Ikeda-Saito, M.; Yonetani, T. "Frontiers of Biological Energetics"; Academic Press: New York, 1978; Vol. 2, pp 1011–1016.

(53) The use of g should not be confused with the g value. g is retained to be consistent with the notation of Tovrog et al.[10]

Table VI. ^{17}O Hyperfine Data and Spin Densities of $B_{12r}O_2$

	a_O[a]	$T_{x'}^O$ [a]	$T_{y'}^O$ [a]	$\rho(s)$[b]	$\rho(p_{x'})$[b]	$\rho(p_{y'})$[b]
O_α	−31.2 ± 6	−121.2 ± 16, 60.6 ± 8, 60.6 ± 8	−14.9 ± 9, 29.8 ± 17, −14.9 ± 9	0.007	0.42 ± 0.05	−0.10 ± 0.06
O_β	−38.6 ± 6	−143.6 ± 16, 71.8 ± 8, 71.8 ± 8	−18.6 ± 9, 37.2 ± 17, −18.6 ± 9	0.008	0.50 ± 0.05	−0.13 ± 0.06

[a] Hyperfine coupling constants in megahertz. [b] Atomic orbital coupling from ref 59.

constant of aryl nitroso compounds for an estimate of U_{Co-O},[10] α'^2 has to be zero, i.e., complete electron transfer takes place.

These results demonstrate that in the case of $B_{12r}O_2$ the superoxide formulation with predominant π-back-bonding and a pronounced electron transfer from cobalt to dioxygen may adequately describe the anisotropic part of the experimentally observed cobalt hyperfine tensor.

A Co(III) oxidation state would also be in agreement with the Co(III)-type UV–vis spectrum of $B_{12r}O_2$ in methanol at temperatures below −50 °C.[15] On the basis of IR spectra of the oxygen adduct of CoSMDPT in absence and presence of 2,2,2-trifluoroethanol, Drago et al.[54] presented arguments to interpret O_2 bonding as predominantly not ionic. Transfer of this bonding picture to $B_{12r}O_2$, however, appears not compelling. Since the symmetry defined by the magnetic parameters of $B_{12r}O_2$ is only C_1, extensive mixing of cobalt 3d orbitals may take place. Drago et al.[1b,c] pointed to this fact and qualified their calculated values for the electron transfer as being semiquantitative. Nevertheless, the spin-pairing model introduced by these authors[1,10] allows a chemically significant insight into the bonding problems arising in cobalt oxygen carriers.

^{17}O hyperfine structure has been measured for both the terminal (O_β) and the adjacent (O_α) oxygen nucleus. The low-temperature ^{17}O hyperfine tensors given in Table II are composed of

$$A^O = a_O + T_{x'}^O + T_{y'}^O$$

where a_O is the isotropic hyperfine coupling and $T_{x'}^O$ and $T_{y'}^O$ denote the dipolar hyperfine tensors attributed to $p_{x'}$ and $p_{y'}$ oxygen orbitals. Values for a_O, $T_{x'}^O$ and $T_{y'}^O$ and the spin densities in the corresponding orbitals are given in Table VI. From the negative values of a_O and the parallel components of $T_{x'}^O$, *positive* spin density in the 2s and $p_{x'}$ orbital results from $g(^{17}O) < 0$. The large values found for $p_{x'}(O_\alpha)$ and $p_{x'}(O_\beta)$ demonstrate that the unpaired electron is mainly located on the dioxygen moiety. The small negative spin density in the $p_{y'}$ orbitals may be produced via spin polarization. The total spin density on O_2 is found to $\rho_{O_2} = 0.7 \pm 0.1$, and hence a spin density $\rho_{corrin} = 0.3 \pm 0.1$ is expected on cobalt and the corrin system. Similar ^{17}O hyperfine coupling constants have been observed for the monomeric Co–O_2 adducts Co(bzacen)(py)(O_2),[55] $[Co^{III}(NH_3)_nO_2^-]^{2+}$ within a $Co^{III}Y$ zeolite,[56] and oxycobaltomyoglobin.[44]

Dynamics of the Co–O_2 Fragment. In order to interpret the striking temperature dependence of the magnetic parameters of $B_{12r}O_2$, three different models will be considered.

Thermodynamic model: $B_{12r}O_2$ is assumed to possess two distinct states, A ⇄ B, characterized by the low- and high-temperature parameters given in Tables II and III. These two states are assumed to be in equilibrium (A ⇄ B) with a high interconversion rate, so that the system behaves according to the fast-exchange limit with respect to the EPR time scale at all temperatures. This latter assumption is suggested by the lack of observable coalescence of the EPR lines of $B_{12r}{}^{16}O_2$. In such a model the molar fractions x_A, x_B fulfill the relation ($x_A + x_B = x_0$):

$$K = x_B/x_A = \frac{x_B/x_0}{1 - x_B/x_0} = \frac{\xi}{1 - \xi} \quad (8)$$

Denoting the temperature-dependent direction cosines matrix of the **g** tensor by $D(T)$, the relation

$$D(T)g(T)\tilde{D}(T) = \xi(T)D_A g_A \tilde{D}_A + (1 - \xi(T))D_B g_B \tilde{D}_B \quad (9)$$

should hold, where $g(T)$ denotes the temperature-dependent (diagonal) **g** tensor and g_A, D_A, g_B, and D_B (given in Tables II and III) the corresponding low- and high-temperature values. In the temperature interval considered (Ulich's approximation)[57]

$$K(T) \approx \exp(-\Delta H^\circ/RT + \Delta S^\circ/R) \quad (10)$$

The observed temperature dependence of **g** and **D** then allows determination of ΔH° and ΔS° provided eq 10 is satisfied by the empirical data. Regression of the usual van't Hoff plot leads to $\Delta H^\circ \approx -6 \pm 1$ kcal/mol and $\Delta S^\circ \approx -24 \pm 4$ cal/(mol·K). The value of ΔH° relates closely to reaction enthalpies of intermolecular hydrogen bonds and conformation interconversions. The reaction entropy appears comparatively large and indicates that crystal water molecules will be involved in the process. This conclusion is supported by thermodynamic data of the crystal water[15] and the kinetics of the $B_{12r}O_2$ formation discussed above. The value $g_{z'} = 2.049$ for the high-temperature state B is unusually small for a localized Co–O_2 fragment as predicted in this model. A similar value ($g_{z'} = 2.054$), however, has been observed in Co^{II}(tspc)–apomyoglobin at −165°C by Ruzic et al.[48] On the other hand, the thermodynamic model does not explain the independence of the z' axis direction on temperature and the equality of the traces of g_A and g_B.

Crystal-field model: $B_{12r}O_2$ is subject to the crystal field of the B_{12b} host molecules and the crystal water. In view of the complexity of the B_{12b} crystal structure it might be argued that the crystal field experienced by the dioxygen adduct is temperature dependent. This would induce a continuous variation of the nuclear configuration of the dioxygen molecule with changing temperature and would thus alter their magnetic parameters. Within this model the pronounced temperature dependence of the **g** and $\mathbf{A}^{Co}$ tensors would again imply cooperation of crystal water molecules. Hori et al.[45] assume that such variations of the crystal field are responsible for the great changes observed in the EPR spectra of oxycobaltomyoglobin in going from ambient ($g_{z'} = 2.056$) to cryogenic temperatures ($g_{z'} = 2.085$). This crystal-field model is not in contradiction with any of the available experimental data. The constancy of the traces of **g** and $\mathbf{A}^{Co}$ with temperature ($g_{iso}(-160\ °C) = 2.032 \pm 0.009$, $g_{iso}(40\ °C) = 2.027 \pm 0.010$, $A_{iso}^{Co}(-160\ °C) = -38 \pm 7$ MHz, $A_{iso}^{Co}(40\ °C) = -37 \pm 10$ MHz), however, again has to be considered accidental. Moreover, the small ^{17}O hyperfine splittings at 40 °C would not fit with data of comparable complexes.

Dioxygen disorder model: This model explains the temperature dependence of the **g** principal values depicted in Figure 9, a and b, by a thermal motion of the dioxygen fragment. Rotation around the Co–O_α axis can be excluded because for this motion the averaged **g** tensor would be axial with $g_\parallel^{av} = 2.023$ along the complex normal and $g_\perp^{av} = 2.036$, in contradiction to the experimental data. A second type of motion is rapid "wobbling", defined by a restricted random walk of O_β within a cone along the low-temperature O_α–O_β direction. This kind of motion would increase $g_{x'}$ and $g_{y'}$ and decrease $g_{z'}$ but would conserve the directions of all the principal axes of **g**. The third motion involves restricted oscillation of O_β in a plane spanned by $\overline{O_2O_\beta}$ and a vector x'' perpendicular to this direction. The general formula for the motion-averaged diagonal elements of the **g** tensor for such an oscillation are given by eq 11a–c, where $g_{x'}$, $g_{y'}$, and $g_{z'}$ denote

(54) Drago, R. S.; Cannady, J. P.; Leslie, K. A. *J. Am. Chem. Soc.* **1980**, *102*, 6014–6019.
(55) Getz, D.; Melamud, E.; Silver, B. L.; Dori, Z. *J. Am. Chem. Soc.* **1975**, *97*, 3846–3847.
(56) Vansaut, E. F.; Lunsford, J. H. *Adv. Chem. Ser.* **1973**, *121*, 441–447.
(57) Kortüm, G. "Einführung in die Chemische Thermodynamik"; Verlag Chemie: Weinheim/Bergstr., West Germany, 1972.

$$g_{x'}^{av} = \tfrac{1}{2}\cos^2\epsilon[(g_{x'}\cos^2\eta + g_{y'}\sin^2\eta)(1+P) + g_{z'}(1-P)] + \sin^2\epsilon(g_{x'}\sin^2\eta + g_{y'}\cos^2\eta) - 2\sin\epsilon\cos\epsilon\sin\eta\cos\eta(g_{x'} - g_{y'})Q \quad (11a)$$

$$g_{y'}^{av} = \tfrac{1}{2}\sin^2\epsilon[(g_{x'}\cos^2\eta + g_{y'}\sin^2\eta)(1+P) + g_{z'}(1-P)] + \cos^2\epsilon(g_{x'}\sin^2\eta + g_{y'}\cos^2\eta) + 2\sin\epsilon\cos\epsilon\sin\eta\cos\eta(g_{x'} - g_{y'})Q \quad (11b)$$

$$g_{z'}^{av} = \tfrac{1}{2}[(g_{x'}\cos^2\eta + g_{y'}\sin^2\eta)(1-P) + g_{z'}(1+P)] \quad (11c)$$

the g principal values of the rigid low-temperature configuration. ϵ and η describe the angle between the principal axis of $g_{x'}$ and x'' and the direction of the axis of $g_{x'}^{av}$, respectively (see Figure 9d). $P = \sin\alpha\cos\alpha/\alpha$ and $Q = \sin\alpha/\alpha$, where α denotes the half-amplitude of the restricted oscillation. For $\eta = \epsilon = 0$, eq 11a-c reduce to the expressions given by Van et al.[58] Both types of motions, wobbling or oscillation of O_β, are not able to adequately describe the experimental data. Wobbling cannot explain the observed rotation of $g_{x'}$ and $g_{y'}$ by $\eta = 25°$ around $\overline{O_\alpha O_\beta}$. On the other hand, the small room-temperature value of $g_{z'}^{av} = 2.049$ leads to an unreasonably large angle α for the oscillation model. In addition, for a quantitative calculation of the disorder of O_β a distribution function had to be introduced.

The motion of O_β in $B_{12r}O_2$ will therefore qualitatively be best described as an oscillation in a plane inclined to ring C, which is superimposed by a certain amount of wobbling. This type of disorder of O_β is illustrated in Figure 9d. Such a motion of the dioxygen fragment explains both observations, the strong decrease of the largest diagonal element of $\mathbf{g}$ and the conservation of the traces of $\mathbf{g}$ and $\mathbf{A}^{Co}$ with increasing temperature. It also causes a considerable decrease of $A_{x'}^{17O}$. Similar disorder of the σ-bonded O_2 molecule in cobalt dioxygen adducts at ambient temperature have been observed in a number of X-ray investigations.[5,6,7,8,51] The different types of disorder models proposed in these studies are summarized in Table V.

Acknowledgment. We express our gratitude to Sandoz AG, Basle, for financial support. We also thank Prof. J. H. Ammeter for the opportunity to measure Q-band spectra on his spectrometer. Furthermore we are grateful to Dr. M. Rudin for helpful discussions, to W. Businger for technical assistance with the high-pressure experiments, to Dr. T. Dschen for his data processing program PACKAGE, and to C. Rey for the preparation of the single crystals.

Registry No. $B_{12r}O_2$, 12581-61-2.

(58) Van, S. P.; Birrell, G. B.; Griffith, O. H. *J. Magn. Reson.* **1974**, *15*, 444-459.
(59) Morton, J. R. *Chem. Rev.* **1964**, *64*, 453-471.

Mixed-Valence Chemistry of Adjacent Vanadium Centers in Heteropolytungstate Anions. 1. Synthesis and Electronic Structures of Mono-, Di-, and Trisubstituted Derivatives of α-$[P_2W_{18}O_{62}]^{6-}$ [1]

Subhash P. Harmalker, Michele A. Leparulo, and Michael T. Pope*

Contribution from the Department of Chemistry, Georgetown University, Washington, D.C. 20057. *Received November 29, 1982*

Abstract: Heteropolytungstates α-$[P_2(W,V)_{18}O_{62}]^{n-}$ containing respectively one (α_2-V), two (V_2), and three (V_3) vanadium atoms in one of the two equivalent M_3O_{13} "caps" of the α-$P_2W_{18}O_{62}$ structure have been synthesized and characterized by ^{31}P and ^{51}V NMR spectroscopy, electrochemistry, and optical and ESR spectroscopy of reduced and mixed-valence derivatives. The latter species show 15-line (V_2), 22-line (V_3), and 36-line (V_3) ESR spectra at 300-350 K, which collapse to "normal" eight-line spectra at <100 K. The complexes therefore are class II mixed-valence species with rapidly hopping electrons at room temperature ($k = 1.1 \times 10^{10}$-3.3×10^{11} s^{-1}) and trapped but partially delocalized electrons ($J = 0.074$-0.135 eV) below ca. 100 K. At 107-157 K, electron transfer in $[P_2W_{15}V^{IV}V_2^{V}O_{62}]^{10-}$ is virtually activationless ($E_a = \sim 0.01$ eV). ESR spectra of mixed-valence V_2 and protonated V_3 species are identical at low temperatures and show superhyperfine structure consistent with 5-10% electron delocalization on to the neighboring V(V) atoms. On the basis of the analysis of the intervalence bands of the three mixed-valence complexes, the high-temperature activation energy, E_{th}, is greater for the trinuclear species than for the binuclear as predicted from a recent theoretical model. The stereoisomer of α_2-V (α_1-$[P_2W_{17}VO_{62}]^{8-}$) has also been prepared and characterized. Separation of a mixture of α_1- and α_2-isomers has been achieved by chromatography on modified Sephadex.

It is generally agreed that partial reduction of heteropolymolybdate and -tungstate anions leads to mixed-valence complexes (heteropoly blues) that belong to class II of the Robin-Day scheme.[2,3] Such complexes are therefore described in terms of trapped electrons (Mo^{5+} or W^{5+} centers) that undergo thermal or optical excitation to neighboring Mo^{6+} or W^{6+} sites. A satisfactory quantitative description of these complexes must include magnitudes of activation energies, electron-transfer rates, and

(1) From the Ph.D. Theses of S.P.H. (Georgetown University, 1982) and M.A.L. (Georgetown University, in preparation). A preliminary account of some of this work has been published: Harmalker, S. P.; Pope, M. T. *J. Am. Chem. Soc.* **1981**, *103*, 7381.
(2) Robin, M. B.; Day, P. *Adv. Inorg. Chem. Radiochem.* **1967**, *10*, 247. Day, P. *Int. Rev. Phys. Chem.* **1981**, *1*, 149.
(3) Prados, R. A.; Pope, M. T. *Inorg. Chem.* **1976**, *15*, 2547. Che, M.; Fournier, M.; Launay, J. P. *J. Chem. Phys.* **1979**, *71*, 1954. Launay, J. P.; Fournier, M.; Sanchez, C.; Livage, J.; Pope, M. T. *Inorg. Nucl. Chem. Lett.* **1980**, *16*, 257. Sanchez, C.; Livage, J.; Launay, J. P.; Fournier, M.; Jeannin, Y. *J. Am. Chem. Soc.* **1982**, *104*, 3194.

0002-7863/83/1505-4286$01.50/0